

NUMERICAL SIMULATIONS OF IMPULSIVELY EXCITED ACOUSTIC-GRAVITY WAVES IN A STELLAR ATMOSPHERE

M. GRUSZECKI

Centre for Fusion, Space and Astrophysics
Department of Physics University of Warwick
Coventry CV4 7AL, United Kingdom

K. MURAWSKI

Group of Astrophysics and Gravity Theory, Institute of Physics
Maria Curie-Skłodowska University
Radziszewskiego 10, 20-031 Lublin, Poland

A.G. KOSOVICHEV, K.V. PARCHEVSKY

W.W. Hansen Experimental Physics Laboratory, Stanford University
Stanford, CA 94305-4055, USA

T. ZAQRASHVILI

Georgian National Astrophysical Observatory
Abastumani Astrophysical Observatory
Kazbegi Ave. 2a, Tbilisi 0160, Georgia

(Received December 13, 2010; revised version received April 15, 2011)

We aim to consider impulsively-generated non-linear acoustic-gravity waves in a gravitationally-stratified stellar atmosphere. Two-dimensional hydrodynamic equations are solved numerically for an ideal plasma with a realistic temperature profile. The numerical results show that an initial pulse in vertical velocity excites a leading wave front which is followed by a dispersive wake, oscillating with a period close to the acoustic cut-off period P_{ac} of the chromosphere. Impulses launched deeper within a low region of the stellar atmosphere result in a wake of smaller P_{ac} . They form quasi-periodic shocks traveling from the chromosphere to the corona. The interaction of the secondary (“rebound”) shocks with the chromosphere-corona transition region generates vortex motions, which may play important role the transition region dynamics.

DOI:10.5506/APhysPolB.42.1333

PACS numbers: 95.30.Qd, 96.60.Hv, 96.60.P-, 96.60.Ly

1. Introduction

Waves play an important role in the dynamics of the stellar atmosphere. For instance, they are believed to carry energy from the photosphere into the solar corona and contribute to coronal heating as well as to generation of the solar wind. In a magnetic-free medium these waves represent acoustic-gravity waves.

In a one-dimensional uniform medium an initial localized perturbation results in two pulses traveling in the opposite directions and leaving behind them an undisturbed medium. Propagation in a gravitationally stratified atmosphere is more complex. The waves become dispersive with the longer wavelengths exhibiting faster (slower) phase (group) speeds. A localized perturbation results in a leading wave front that is followed by a dispersive wave oscillating with a frequency asymptotically approaching the acoustic cut-off frequency. In an inhomogeneous medium the waves can experience scattering and reflection. This can take place when a wave propagates into a region of a different characteristic wave speed, *e.g.* in the transition region between the chromosphere and corona.

In the linear approximation, the one-dimensional propagation of waves in the vertical direction corresponds to acoustic waves alone, and is governed by the Klein–Gordon-type equation [1]. In the case of non-vertical wave propagation, the acoustic and gravity waves are coupled, and their evolution is described by 4th order wave equation [2].

In the stellar atmosphere, the role of gravity depends on the ratio between the wavelength and the gravitational scale-height, Λ . In the solar corona, Λ is large and the influence of gravity is small. However, in the solar photosphere Λ is relatively small, and the effect of gravity is important. The transition region lying between the photosphere and the corona is extremely complicated, as the stratification effects are most pronounced there. In addition, the solar waves become non-linear in the upper chromosphere and corona. Therefore, the wave propagation in the solar atmosphere is difficult to model analytically, and numerical treatment is required.

Initial numerical simulations of one-dimensional waves in a stratified atmosphere were obtained by Stein and Schwartz [3], and Kneer and Nakagawa [4]. They found formation of a secondary impulse in the wake of the initial shock, and related this to the oscillations described by Lamb [1]. Kosovichev and Popov [5] carried out numerical simulations of impulsively excited waves in a model that included both the chromosphere and corona, and found the effect of quasi-periodic shocks traveling through the transition region into the corona. The process lasted for about an hour after the initial impulse. The model was applied to non-linear oscillations of the solar atmosphere [6]. Goode *et al.* [7] and Restaino *et al.* [8] compared the numerical

simulations with observations, and found evidence for the oscillatory wakes caused by impulsive events. Hollweg [9] suggested that the phenomenon of the quasi-periodic (“rebound”) shocks can provide the mechanism for solar spicules. However, the subsequent simulations (*e.g.* [10]) showed that the maximum height of spicules in this model does not exceed $\sim 7\text{--}8$ Mm, and that a magnetic field driving is needed to explain higher spicules and macrospicules [11]. For a recent discussion of spicule observations and models see Pasachoff *et al.* [12] and Murawski and Zaqarashvili [13].

Numerical simulations using a high-accuracy code were carried out in one dimension by Bryson *et al.* [14], who confirmed that the solar atmosphere responds to forcing at the solar surface with several strong shocks, which lift the transition region well into the corona. We aim to extend the 1D simulations to their 2D equivalence. Instead of the forcing term that was used by Bryson *et al.* [14] for wave excitation we consider waves triggered impulsively.

This paper is organized as follows. The numerical model is described in Sec. 2. The numerical results are presented and discussed in Sec. 3. This paper is concluded by a summary of the main results in Sec. 4.

2. A numerical model

2.1. Hydrodynamic equations

Our model system is a gravitationally-stratified stellar atmosphere. We restrict ourselves to the hydrodynamic equations, in which the radiation and thermal conduction are neglected. Below we write hydrodynamic equations in conservative form:

$$\frac{\partial \varrho}{\partial t} + \nabla \cdot (\varrho \mathbf{V}) = 0, \quad (1)$$

$$\frac{\partial(\varrho \mathbf{V})}{\partial t} + \nabla \cdot (\varrho \mathbf{V} \otimes \mathbf{V}) + \nabla p = -\varrho \nabla \phi, \quad (2)$$

$$\frac{\partial(pE)}{\partial t} + \nabla \cdot [\varrho \mathbf{V}(E + p/\varrho)] = -\varrho \mathbf{V} \cdot \nabla \phi. \quad (3)$$

Here ϱ is the mass density, $\mathbf{V} = [V_x, V_y, V_z]$ is the flow velocity, p is the thermal pressure, $\gamma = 5/3$ is the adiabatic index, ϕ is the gravity potential and E is the total energy. We limit our modeling to a 2D (x – z) environment, in which all plasma quantities are invariant with y ($\partial/\partial y = 0$).

2.2. Initial configuration

2.2.1. The equilibrium

We assume that at equilibrium the stellar atmosphere is static ($\mathbf{V} = 0$). Then, the pressure gradient force is balanced by the gravity, that is

$$-\frac{\partial p_e}{\partial z} - \varrho_e g = 0. \quad (4)$$

Here, the subscript e corresponds to the equilibrium and z denotes height. Using the equation of state and the z -component of hydrostatic pressure balance indicated by Eq. (4), we express equilibrium gas pressure $p_e(z)$ and mass density $\varrho_e(z)$ as

$$p_e(z) = p_0 \exp\left(-\int_0^z \frac{dz'}{\Lambda(z')}\right), \quad (5)$$

$$\varrho_e(z) = \frac{p_e(z)}{g\Lambda(z)}. \quad (6)$$

Here,

$$\Lambda(z) = k_B T_e(z)/(mg) \quad (7)$$

is the pressure scale-height, $T_e(z)$ is the equilibrium temperature and p_0 is the gas pressure at the reference photospheric level, chosen here as $z = 0$.

We adopt an equilibrium temperature profile $T_e(z)$ for the stellar atmosphere that is close to the VAL-C atmospheric model of Vernazza *et al.* [15]. This profile is displayed in Fig. 1, left top panel. With the use of Eqs. (5) and (6) we obtain the gas pressure and mass density profiles (Fig. 1, right top and bottom panels).

It is noteworthy that the equilibrium plasma density and pressure vary by up to 8 orders of magnitude in the simulation region. Such large variations cause a formidable challenge for numerical methods.

2.3. Vertically propagating acoustic waves of small amplitude

For interpretation of the simulation results, it is instructive to consider first vertically propagating waves. As gravity waves are unable to propagate along \mathbf{g} , this case corresponds to acoustic waves only. Small amplitude perturbations of the equilibrium described by Eqs. (5) and (6) are governed by a Klein–Gordon-type equation (*e.g.* [1, 5, 16])

$$\frac{\partial^2 Q}{\partial t^2} - c_s^2 \frac{\partial^2 Q}{\partial z^2} = -\Omega^2(z)Q. \quad (8)$$

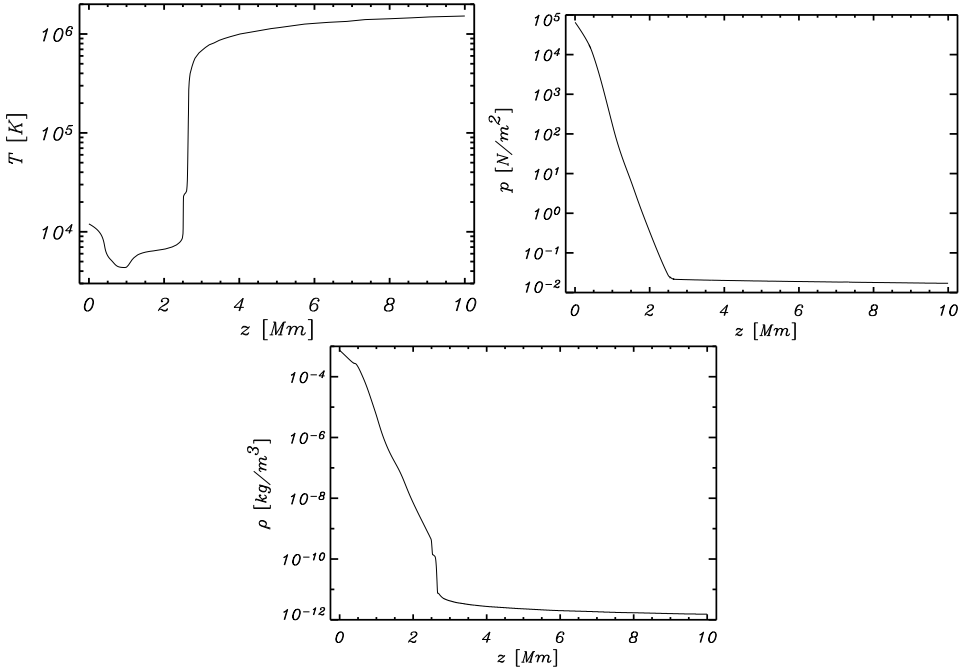


Fig. 1. Equilibrium profiles of temperature (left top panel), gas pressure (right top panel) and mass density (bottom panel) for a gravitationally-stratified stellar atmosphere.

Here,

$$Q(z, t) = \sqrt{\frac{\varrho_e(z)c_s^2(z)}{\varrho_e(0)c_s^2(0)}} V_z(z, t), \quad \Omega^2(z) = \frac{c_s^2(z)}{4\Lambda^2(z)} \left(1 + 2\frac{\partial\Lambda}{\partial z} \right), \quad (9)$$

is the squared acoustic cut-off frequency,

$$c_s(z) = \sqrt{\frac{\gamma p_e(z)}{\varrho_e(z)}} \quad (10)$$

is the sound speed. It is noteworthy that V_z is amplified with height. From Eq. (9) we get

$$|V_z| \sim p_e(z)^{-1/2} |Q|. \quad (11)$$

Hence, for bounded $|Q|$, $|V_z|$ grows like $e^{z/(2\Lambda)}$, giving an e-folding distance of $2\Lambda(z)$. In the photosphere $\Lambda = 125$ km. As a result, a 1 km s^{-1} wave amplitude in the photosphere would grow to the sound speed in about 500 km, leading to a shock in the chromosphere.

For an isothermal atmosphere $T(z) = \text{const.}$ and from Eq. (8) we get the dispersion relation

$$\omega^2 = k_z^2 c_s^2 + \Omega_{\text{ac}}^2. \quad (12)$$

Hence we infer that wave propagation occurs only if a wave frequency ω is higher than an acoustic cut-off frequency Ω_{ac} (*e.g.* [16])

$$\Omega_{\text{ac}} = \frac{\gamma g}{2c_s}. \quad (13)$$

Under the photospheric conditions a corresponding wave period $P_{\text{ac}} = 2\pi/\Omega_{\text{ac}}$ is about 200 s. Thus, pure harmonic waves are propagating when their wave period, P , is such that $P < P_{\text{ac}}$. As a result, in the photosphere we have wave propagation for $P < 200$ s. Larger wave period waves are evanescent. However, in the case of impulsively excited waves there is an effect of apparent propagation of waves with periods longer than P_{ac} [7]. In the stellar corona, $P_{\text{ac}} \sim 90$ min.

In the case sound waves are triggered impulsively a wave front results from the initial pulse. Behind this wave front an oscillating wake appears [1]. This wake oscillates with a frequency asymptotically approaching Ω_{ac} , and its amplitude declines in time [5, 17].

2.4. Nonlinear perturbations

We generate waves in the stellar atmosphere, that is described by Eqs. (5)–(7), by launching initially, at $t = 0$, a pulse in z -component of velocity, V_z *i.e.*

$$V_z(x, z, t = 0) = A_V \exp \left[-\frac{(x - x_0)^2}{w_x^2} - \frac{(z - z_0)^2}{w_z^2} \right]. \quad (14)$$

Here, the maximum amplitude of the initial pulse is chosen and hold fixed: $A_V = 3.3 \times 10^3 \text{ m s}^{-1}$.

3. Numerical results

Equations (1)–(3) are solved numerically using the code `RAMSES` [18, 19]. This code implements a second-order unsplit Godunov solver with various slope limiters and Riemann solvers as well as Adaptive Mesh Refinement (AMR). We use the Monotonized Central slope limiter, the Roe and LLF Riemann solver in MUSCL-Hancock scheme (*e.g.* [20]). We set the simulation box as $(0, L) \times (0, L)$, with $L = 10$ Mm. Open boundary conditions for all perturbed plasma quantities are imposed at the left- and right-sides of the simulation region, while at $z = 0$ and $z = L$ all quantities are fixed to

their equilibrium values. In our studies we use AMR grid with a minimum (maximum) level of refinement blocks set to 5 (11). The refinement strategy is based on controlling numerical errors in a gradient of mass density. Initially, at $t = 0$, we cover the simulation region by 3×10^6 numerical cells. Such setting results in an excellent resolution of steep spatial profiles and significantly reduces numerical diffusion within the simulation region.

3.1. A wave-front

We consider first the case of a wave-front that is independent of z . We choose $w_x = 0.7$ Mm and $w_z \rightarrow \infty$ (Eq. 14). It is noteworthy that this wave-front does not evolve in time; at two consecutive times profiles of $V_z(x)$ are essentially identical (Fig. 2). Such scenario results from the fact that the hydrodynamic equations include both vortex and acoustic solutions [21]. The vorticity perturbations have zero frequency ($\omega = 0$) and can be easily distinguished from acoustic solutions in simple static medium. The considered initial profile of velocity corresponds to the vortex perturbations (as there is no initial pressure perturbation). Therefore such perturbation does not evolve in time. This scenario takes place in simple and complex cases. For instance, the phenomenon of the nonlinear vortex adjustment was discussed by means of numerical simulations in the context of differentially rotating Keplerian discs [22].

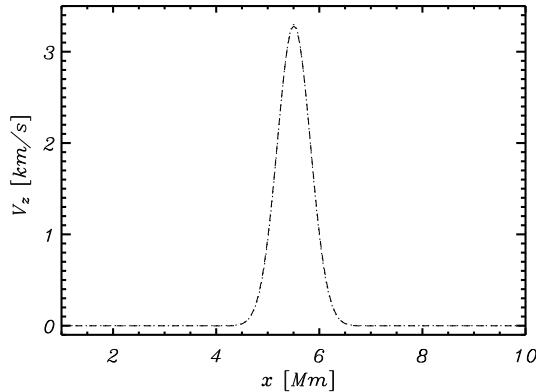


Fig. 2. Profiles of $V_z(x, z = 5 \text{ Mm}, t)$ at $t = 0$ s (dotted line) and $t = 30$ s (dashed line) for the initial pulse of Eq. (14) with $w_x = 0.7$ Mm, $w_z \rightarrow \infty$ and $x_0 = 5$ Mm.

We discuss now the case of a vertically propagating wave-front that is triggered by the initial pulse with $w_x \rightarrow \infty$, $w_z = 0.35$ Mm in Eq. (14). We launch the initial pulse at two different heights: (a) within the photosphere and (b) in the stellar corona. Figure 3 illustrates time-signatures of the propagating wave-front. These time-signatures were made by collecting a

signal in time along the z -direction. We consider first the case of the initial pulse that is launched within the stellar corona (Fig. 3, left panel). This initial pulse spreads shortly afterwards into two counter-propagating waves. These waves propagate upwards with the sound speed of the stellar corona. At $t \simeq 20$ s it leaves the simulation region through the top boundary. The waves which propagate downwards reach the transition region at $t \simeq 40$ s. As the sound speed experiences a sudden fall-off there a significant part of this wave is reflected back into the corona.

The above scenario differs in the case of the initial pulse is launched below the transition region (Fig. 3, right panel). The initial perturbation results in a leading wave front that propagates at the local sound speed. Behind this front is trailed an oscillating wake.

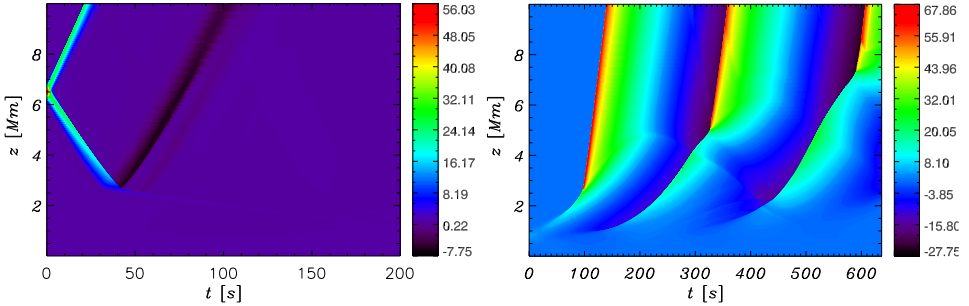


Fig. 3. Time-height diagram of V_z (color scale: in km s^{-1}), for the case of the horizontally uniform pulse of Eq. (14) with $w_x \rightarrow \infty$ and $w_z = 0.35$ Mm. Left panel: $z_0 = 6.5$ Mm; right panel: $z_0 = 0.8$ Mm.

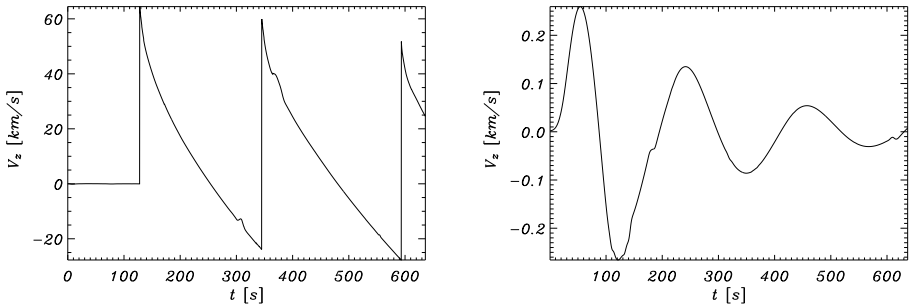


Fig. 4. Variations of $V_z(x = 5 \text{ Mm}, z, t)$ with time at $z = 7.75$ Mm (left panel) and $z = 0.13$ Mm (right panel) for the case of Fig. 3 (right panel).

Figure 4 illustrates variations of V_z (Fig. 3, right panel) in the corona at $z = 6.5$ Mm (left panel) and in the photosphere $z = 0.13$ Mm (bottom panel). Shocks are well seen in the stellar corona (left panel), while in the photosphere the signal corresponds to decaying in time oscillator (right panel). The Fourier power spectrum of z component of velocity V_z (Fig. 5) of the photospheric signal shows a peak at an oscillation period at about 200 s, corresponding to the acoustic cut-off period.

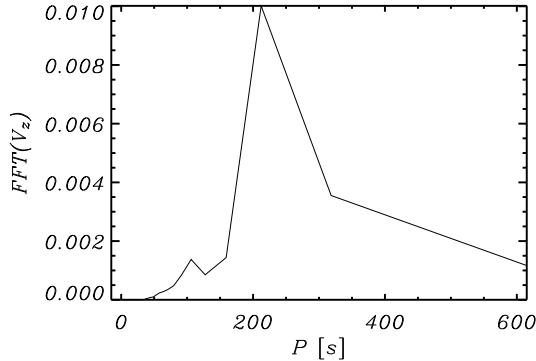


Fig. 5. Fourier power spectrum of the wave signals of Fig. 4.

Figure 6 which illustrates spatial profiles of gas pressure (left panel) and mass density (right panel) at four different moments of time: $t = 0$ s (solid line), $t = 100$ s (dotted line), $t = 300$ s (dashed line) and $t = 590$ s (dash-dotted line). It is well seen that the plasma profiles vary in time, the shocks are well seen in the gas pressure and density profiles (left panel) and the transition region moves upwards (right panel).

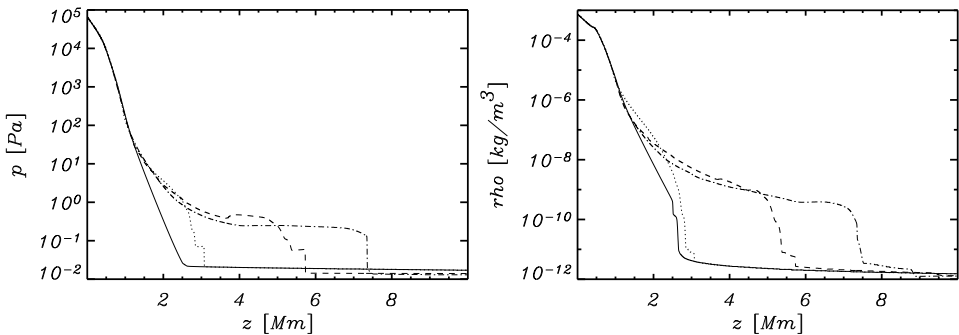


Fig. 6. Vertical profiles of gas pressure (left panel) and mass density (right panel) for the case of Fig. 3 (left panel), $t = 0$ s (solid line), $t = 100$ s (dotted line), $t = 300$ s (dashed line) and $t = 590$ s (dash-dotted line).

3.2. A localized pulse

Now we switch from plane-parallel waves to waves generated by a localized 2D pulse. To excite waves we use a pulse in V_z , which is localized in both x - and z -directions. It triggers both acoustic and gravity waves. We fix a position of this pulse in the middle of the horizontal domain $x_0 = 5$ Mm and at height $z_0 = 0.8$ Mm, and choose its size parameters as $w_x = 1.4$ Mm, $w_z = 0.35$ Mm.

Time variations of $V_z(x = 5 \text{ Mm}, z, t)$ at different heights are displayed in Fig. 7. Similarly to Fig. 3 (right panel) after the first wave front passage a wake is observed. This wake oscillates with a wave period of about 200 s in agreement with our analytical estimation. After $t \simeq 300$ s complex vortex flows are generated in the simulation region (Fig. 7), when the second shock travels through the transition region. Such flows are not observed in the case of the plane-parallel wave front (Fig. 3, right panel).

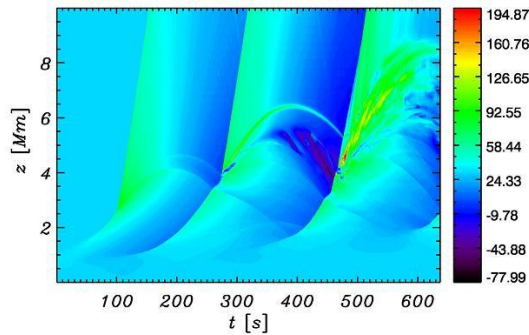


Fig. 7. Time-height diagram of V_z for the case of the initial pulse of Eq. (14) with $w_x = 1.4$ Mm, $w_z = 0.35$ Mm, $x_0 = 5.0$ Mm and $z_0 = 0.8$ Mm (color scale: in km s^{-1}).

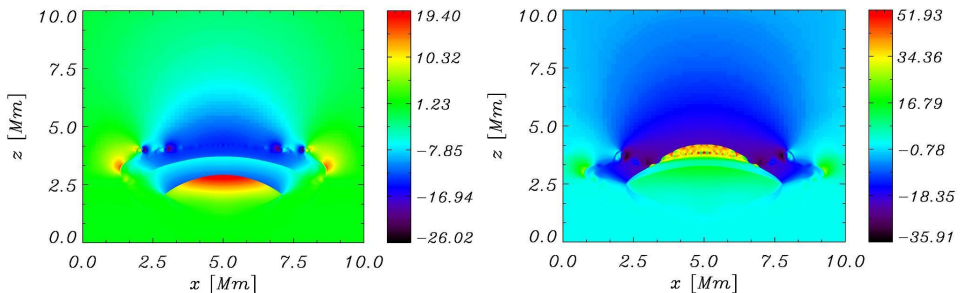


Fig. 8. Profiles of $V_z(x = 5 \text{ Mm}, z)$ for the case of the initial pulse of Eq. (14) with $w_x = 1.4$ Mm, $w_z = 0.35$ Mm, $x_0 = 5$ Mm and $z_0 = 0.8$ Mm at $t = 244$ s (left panel) and $t = 276$ s (right panel) (color scale: in km s^{-1}).

A possible explanation of the vortex flows is that the perturbed transition region experiences subsequent impact from the secondary “rebound” shocks in the wake. When such shocks encounter the perturbed density jump they cause instabilities similar to the Richtmyer–Meshkov (RM) instability [23, 24]. These instabilities are a kind of Rayleigh–Taylor (RT) instabilities [25]. Arendt [26] showed that vortices in a stratified fluid are propagated horizontally. Such propagation is seen in our numerical data (Fig. 8).

4. Conclusions

We have performed numerical simulations of impulsively generated acoustic-gravity waves in a 2D gravitationally stratified stellar atmosphere. Several conclusions result from our simulations:

- (a) our results confirm that an impulsive source in the atmosphere generates a leading wave front and a trailing wake;
- (b) a pulse launched deep within the stellar atmosphere exhibits a tendency to generate shocks; these shocks result from nonlinearities, which become important in the stellar corona where arriving waves reach high amplitudes;
- (c) in the case of initial pulses launched in the stellar corona no substantial wave propagation into the chromosphere is observed; a wave signal reaching the transition region is reflected back into the stellar corona;
- (d) in the case of a localized 2D pulse, the interaction of the secondary shocks with the transition regions results in small-scale vortex flows, which be due instabilities similar to the Richtmyer–Meshkov [23, 24] instability; this phenomenon may play important role in the dynamics of the transition region; this requires further investigation using more realistic numerical simulations.

M.G. and K.M. express their thanks to Sebastian Fromang and Romain Teysier for their assistance in running the **RAMSES** code. M.G.’s and K.M.’s work was supported by the grant (for years 2007–2010) from the Polish State Committee for Scientific Research (KBN). M.G.’s work was supported by NASA grant NNX07AP61G during his visit to Stanford University and by the Newton International Fellowship NF090143.

REFERENCES

- [1] H. Lamb, *Proc. Lond. Hath. Soc.* **7**, 122 (1909).
- [2] G. Bodo, W. Alkofen, S. Massaglia, P. Rossi, *Astron. Astrophys.* **354**, 296 (2000).
- [3] R.F. Stein, R.A. Schwartz, *Astrophys. J.* **177**, 807 (1972).
- [4] F. Kneer, Y. Nakagawa, *Astron. Astrophys.* **47**, 65 (1976).
- [5] A.G. Kosovichev, I.P. Popov, *Zhurnal Vychislitelnoi Matematiki i Matematicheskoi Fiziki* **19**, 1253 (1979) (Eng. trans. *USSR Comput. Math. Math. Phys.* **19**, 168 (1980)).
- [6] A.G. Kosovichev, Y.P. Popov, *Bull. Crimean Astrophys. Obs.* **63**, 15 (1981).
- [7] P.R. Goode, D. Gough, A.G. Kosovichev, *Astrophys. J.* **387**, 707 (1992).
- [8] S.R. Restaino, R.T. Stebbins, P.R. Goode, *Astrophys. J.* **408**, L57 (1993).
- [9] J.V. Hollweg, *Astrophys. J.* **257**, 345 (1982).
- [10] A.S. Andreev, A.G. Kosovichev, *Space Sci. Rev.* **70**, 53 (1994).
- [11] A.S. Andreev, A.G. Kosovichev, *Proc. SOHO Workshop* **373**, 179 (1994).
- [12] Pasachoff, J.M., Jacobson, W.A., Sterling, A.C., *Sol. Phys.* **260**, 59 (2009).
- [13] K. Murawski, T. Zaqarashvili, *Astron. Astrophys.* **519**, A8 (2010).
- [14] S. Bryson, A.G. Kosovichev, D. Levy, *Physica D* **201**, 1 (2005).
- [15] J.E. Vernazza, E.H. Avrett, R. Loeser, *Astrophys. J.* **45**, 635 (1981).
- [16] B. Roberts, *In Proc. SOHO 13 Waves, Oscillations and Small-Scale Transient Events in the Solar Atmosphere: A Joint View from SOHO and TRACE*, Palma de Mallorca, Spain, (ESA SP-547), 1, 2004.
- [17] I.C. Rae, B. Roberts, *Astrophys. J.* **256**, 761 (1982).
- [18] R. Teyssier, *Astron. Astrophys.* **385**, 337 (2002).
- [19] S. Fromang, P. Hennebelle, R. Teyssier, *Astron. Astrophys.* **457**, 371 (2006).
- [20] E. Toro, *Riemann Solvers and Numerical Methods for Fluid Dynamics*, Springer, 1999.
- [21] J. Lighthill, *Waves in Fluids* (Cambridge University Press: Cambridge), 1978.
- [22] G. Bodo *et al.*, *Astron. Astrophys.* **475**, 51 (2007).
- [23] R.D. Richtmyer, *Commun. Pure Appl. Math.* **13**, 297 (1960).
- [24] E.E. Meshkov, *Soviet Fluid Dynamics* **4**, 101 (1968).
- [25] G.I. Taylor, *Math. Phys. Sci.* **201**, 192 (1950).
- [26] S. Arendt, *Geophys. Astrophys. Fluid Dyn.* **68**, 59 (1993).